

# We are IntechOpen, the world's leading publisher of Open Access books Built by scientists, for scientists

6,900

Open access books available

186,000

International authors and editors

200M

Downloads

Our authors are among the

154

Countries delivered to

TOP 1%

most cited scientists

12.2%

Contributors from top 500 universities



WEB OF SCIENCE™

Selection of our books indexed in the Book Citation Index  
in Web of Science™ Core Collection (BKCI)

Interested in publishing with us?  
Contact [book.department@intechopen.com](mailto:book.department@intechopen.com)

Numbers displayed above are based on latest data collected.  
For more information visit [www.intechopen.com](http://www.intechopen.com)



---

# Nanostructuring of Material Surfaces by Laser Ablation

---

Cinthya Toro Salazar, María Laura Azcárate and  
Carlos Alberto Rinaldi

Additional information is available at the end of the chapter

<http://dx.doi.org/10.5772/62638>

---

## Abstract

Irradiation of materials such as iron and silicon with single nanosecond laser pulses produces nanostructures on its surfaces. Nevertheless, the deposition before irradiation of thin films on the surface of the silicon wafers can modify the shapes of these structures. Upon laser irradiation, different effects are produced on the surfaces of monocrystalline silicon wafers coated with a thin film of  $\text{Si}_3\text{N}_4$  than on that of bare ones. After irradiation with a Nd:YAG laser pulse of 532 nm, the coated silicon surface presents a nanostructure that, due to its hydrophobic behavior, can be used for biological applications such as cell growth. On the other hand, the nanostructures formed on the surface of metals, such as iron, make them more resistant to oxidation processes by changing their oxidation potentials.

**Keywords:** nanosecond laser ablation, nanoparticles, surface roughness, nanostructures, laser micromachining

---

## 1. Introduction

The surface nanostructuring and the generation of nanoparticles by laser ablation with nanosecond lasers are subjects that have gained importance in the last 15 years [1]. These issues were present since the early experiments with pulsed lasers because they are inherent to pulsed laser interaction with matter, and researchers have made great efforts to get rid of them. In laser ablation micromachining, these effects are known as HAZ (heat affected zone) and are undesirable [1, 3]. It was not until the explosive spring forth of nanotechnology in technological applications in several areas such as medicine and microelectronics among many others that the appearance of different nanostructures in a wide variety of materials started to be reported in the literature.

In this chapter, we will present a review of the nanostructures found by our research group during the quality control of the surfaces of micromachined devices. On the other hand, a method for generating metallic nanoparticles which was developed on the basis of the analysis of the material ejected during the micromachining ablation process will be reported. Nanoparticles were then generated in different media such as air, deionized water, isopropyl alcohol and sodium dodecyl sulfate (SDS) solution. Preliminary results of the generation of Fe@Au nanoparticles (core-shell nanoparticles) will be also discussed.

A brief summary of the fundamentals of laser ablation of solid substrates and of the theory of the resulting ablation plume will be given in the next section. A large variety of studies in this field including basic research and applications have been carried out worldwide by many researchers. However, we will focus on the area of micromachining by laser ablation [1–4].

### 1.1. Laser ablation

The laser ablation mechanism is one of the most complex phenomena observed when laser radiation interacts with a solid material [1]. Ablation may be produced either with pulsed or with intense continuous wave (cw) lasers [1, 3]. For a given type of material, the onset of ablation takes place around a threshold fluence ( $\Phi_{th}$ ), which depends on absorption mechanisms and particular properties of the material, such as its microstructure, its morphology, and the presence of defects as well as on laser parameters (intensity, wavelength, and pulse duration) [1, 2, 5, 6]. When irradiation is performed with several consecutive pulses impinging on the same sample's area,  $\Phi_{th}$  can vary due to the accumulation of defects in the previously irradiated zone. At a given wavelength, the amount of material removed per pulse usually shows a logarithmic increase with fluence in accordance with the Lambert–Beer law. On the other hand, Villagran-Muniz et al. [7] reported heuristic equations to describe the fluence dependence of the amount of removed material per pulse of a given substrate with parameters that can be related to physical properties of the substrate.

In particular, for laser pulse durations larger than 10 ps, the laser beam will also interact with the ablation plume as in the case of 10 ns Nd:YAG lasers. In these conditions, the plume will also absorb and scatter radiation. In consequence, the amount of energy reaching the substrate will be less since part of it will be absorbed by the plasma, generating a hot plasma. This excited plasma will then expand and create shock waves in the molten substrate. Frozen shock waves can be observed in the material when the irradiated zone cools [8]. Another effect produced by the excited plume is the explosion of the remnant molten material, which produces splashes. The expelled liquid will inevitably solidify around the irradiated area together with plume's material condensation. In addition, the rapid generation of large thermal gradients may induce excessive thermal stress and thermoelastic excitation of acoustic waves. These stresses may add hardening work, buckling, or cracking [1] to the response of the material, effects which must be taken into account in each particular application.

However, this is not a general feature of all materials. The dynamics of the laser–matter interaction starts with the electronic excitation and relaxation. For weak electric fields, ionization of an atom occurs when the energy of the incident photon exceeds the binding energy of the valence electron. Thus, unlike metals, in a large variety of materials with valence

bands, such as dielectrics, electrons are not directly excited into the conduction band. In Chapter 8 of reference [1], an extensive explanation of the differences in the absorption processes of between metals and dielectrics is given.

Only the final results of the ablation process and perhaps some insights of the different phenomena that can possibly occur are experimentally observed. When the material's processing involves a laser, the light-matter interaction mechanisms that simultaneously occur will depend on the pulse duration. Thus, the most relevant mechanisms that take place on a substrate according to the laser pulse duration are as follows: material melting with cw and millisecond pulsed lasers, material vaporizing with nanosecond pulses, and finally, sublimation of material with femtosecond pulses [1]. It is worthy to note that short pulses (1 ns–1  $\mu$ s) emitted by lasers with Q-switch devices also reduce the thermal impact on the material.

### *1.1.1. Applications: Nanostructuring and manufacturing of nanoparticles*

Nanomanufacturing was developed in the last decade driven by the nanotechnology progress. Sub-micrometric structures in the irradiation zones or resulting from the ablation plume were observed since the beginning of pulsed lasers applications to materials' processing. However, at that time, these were a problem and many attempts have been made to mitigate them. It was only in the last decade that they were considered useful [9–12].

The large scope of applications of the sub-micrometric structures' with unique properties that have been lately found [13–15] contributed to this change of perspective. Although the manufacture of nanometric structures and particles with pulsed lasers is quite simple and can be applied to a large variety of materials, the phenomena involved are difficult to analyze and simulate, resulting in a theoretical and experimental research field in continuous growth. In particular, in this chapter, we will present a brief overview of the heuristic functions which describe the laser fluence dependence of the removed material in laser ablation processes of different substrates as well as the nanostructures and nanoparticles found in the analysis with an electronic microscope of the quality of micromachined devices and of the material ejected in the ablation plume, respectively.

#### *1.1.1.1. Surface modification – nanostructuring*

Nanostructuring by interaction with pulsed lasers is known since the beginning of lasers' applications to machining. However, in recent years, it is an issue that is gaining large importance due to its potential applications in various fields. Different types of nanostructures (NS), named laser-induced periodic surface structures (LIPSS), have been reported. The low spatial frequency LIPSS (LSFL) are characterized by a spatial period  $\Lambda$  of about the laser wavelength ( $\lambda$ ), that is,  $\Lambda \sim \lambda$ . Structures called high spatial frequency LIPSS (HSFL) have a spatial period  $\Lambda$  shorter than the laser wavelength,  $\Lambda \ll \lambda$ . So far, it is accepted that  $\Lambda$  depends on the laser wavelength and on the radiation incidence angle. These LIPSS are generally described by their period  $\Lambda$  and their orientation with respect to the polarization of the laser [9]. However, the origin of the HSFL is still under debate and some theories have been proposed.

Zhang et al. [10] report NS formed with ultrashort lasers pulses (Ti: Sapphire, 1 kHz, 800 nm, 120 fs). They describe the formation of both types of ripples: LSFL and HSFL. They explain that LSFL arise from optical interference effects due to the coherent interaction between the incident radiation and the electromagnetic wave scattered by the surface. Two main mechanisms are proposed for HSFL formation. One is related to the interaction of the laser pulse with the surface plasma produced by the incident laser. The other mechanism is associated to a combination of interference effects and second harmonic generation. For example, they have experimentally found that the period of the ripples decreases with the increase of the laser fluence on the surface. They report ripples generated perpendicular to the laser polarization in the single-crystal superalloy CMSX-4. According to the experiments of these authors, HSFL ( $\Lambda \ll \lambda$ ) are generated from LSFL ( $\Lambda \sim \lambda$ ) with a period about half of the LSFL spatial period. That is, while the period of the crests of LSFL is about the laser wavelength ( $\lambda_L = 800$  nm,  $\Lambda_{LSFL} \sim 760$  nm), that of the HSFL is  $\Lambda_{HSFL} \sim 360$  nm, which is about half the laser wavelength.

NS in silicon were observed in areas up to 100 mm<sup>2</sup> using a versatile laser machining station. Experiences show that the morphology and frequency of the ripples of these structures do not depend either on the focusing geometry, energy, scan rate, polarization, or incident angle of the radiation [11]. It can be thus inferred that laser-based synthesis of nanomaterials is an area that is in its beginnings.

#### 1.1.1.2. Manufacturing of nanoparticles

The manufacture of nanoparticles by pulsed laser ablation is framed within what is known as laser synthesis of nanomaterials (NM). The nanomaterials have extensive applications in electronics, medicine, and energy generation and storage. The physical and chemical properties of these materials strongly depend on their dimensions and shape. The most investigated nanostructures are spheres (nanoparticles (NPs) and “quantum-dots”) and cylinders (nanotubes, nanowires, nanorods). In particular, the nanostructures are made by pulsed laser ablation (PLA). In the PLA of a solid, the NPs produced have the same composition of the solid from which they come. If it takes place in air or vacuum, then thin coatings of NPs formed from the ejected clusters can be generated on the surface. When PLA takes place in a liquid, then a colloidal solution is obtained. On the other hand, there is also evidence that the interaction of the laser radiation with nano- and micro-materials in solutions and/or in suspensions in liquids/gases can produce new structures: nanostructures or alloys, as reported in Chapter 7 of reference [1].

Pulsed laser ablation of materials was introduced with the advent of the ruby laser around 1960 [16]. Since then laser for machining research has been directed to obtain new emission wavelengths, increase the repetition rate and output energy and, of course, decrease the pulse duration, nowadays up to attoseconds ( $10^{-18}$  s). This research was mainly encouraged by the fact that the laser processing is a powerful tool that does not wear during machining and, in addition, does not produce pollution. On the other hand, in PLA, materials are subjected to high temperatures and pressures, giving rise to a very particular chemistry with the production of various compounds of oxides, carbides, and nitrides. Besides, since cooling rate is very high

due to the rapid expansion of the plasma plume, metastable nanomaterials which are difficult to obtain by other techniques can be produced.

PLA is conceptually simple. However, the material removal mechanisms extend over very long intervals, from fs to ms, at least nine orders of magnitude. When the laser is focused on the surface of a dielectric solid, wavelength dependent non-thermal effects take place. When the solids are metals and semiconductors, thermal processes are also present. The mechanisms and the characteristics of the ejected species strongly depend on the parameters of the laser radiation (wavelength, pulse duration, and fluence).

With a nanosecond laser, PLA is basically a photothermal phenomenon. The incident energy excites the electronic and vibrational levels of the substrate and, in consequence, the material is heated, melted, and evaporated in the first 10–100 ps following the pulse arrival. For relatively low fluence radiation ( $\leq 0.3\text{--}1\text{ J/cm}^2$ ), the ejected material, by desorption and evaporation, is mostly atomic size vapor. Then, the resultant vapor plume expands vertically and is ionized by the photons that keep coming. For fluences near the ablation threshold, the amount of ionized material can be calculated by the Saha equation [17]. If the fluence is larger than the ionization threshold, then optical breakdown occurs and the degree of ionization can be estimated from the Saha-Boltzmann equation.

The plasma role during the laser–matter interaction is not yet fully understood and has been discussed over the past two decades. The plasma is composed of a set of atoms and electrons that remain confined in a high energy field. The laser can produce plasma because during a very short time lapse the photons that interact with the atoms of the solid target can strip off about 15 electrons from each atom. Therefore, the photons that arrive after the solid has been vaporized, contribute to increase the degree of ionization [1]. Ionization strongly influences the dynamics of the plume's condensation.

As the laser fluence increases ( $\Phi \geq 10\text{ J/cm}^2$ ), there is a remarkable increase in the amount of ablated material suggesting that a different material ejection mechanism is taking place. Experimentally, it is observed that the removed material consists of a mixture of vapor and micron size droplets ( $\geq 10\text{ }\mu\text{m}$ ). Different mechanisms have been proposed to explain this behavior. Some suggest that temperature gets close to the critical temperature of the material and then a phase explosion follows [1].

In general, it can be said that in the nanomaterials' synthesis, clusters' ejection and gas to particles condensation, take place. The literature reveals that their final size varies within four orders of magnitude [1]. However, Hubental et al. propose a *tailoring* method which can be used to homogenize NPs' size [18].

Regardless of the confinement in which the NPs are generated, certain steps taking place in their formation may be outlined:

1. Vaporization (Nd:YAG lasers) and atomization (fs lasers).
2. Phase explosion.
3. Fragmentation.



4. Mechanical exfoliation or chipping.
5. Hydrodynamic spraying.

The high temperature and density of the ejected material near the target's surface develops a pressure exceeding in several orders of magnitude the atmospheric pressure, leading to an expansion of the vapor. During the adiabatic expansion (occurring at low pressure or vacuum) that follows, the thermal energy is converted into kinetic energy, causing a very fast cooling of the plasma (from  $10^4$  to  $10^5$  K in 1  $\mu$ s for a ns laser). The extreme cooling rate leads the plasma to a supersaturation condition in which nucleation becomes energetically favorable [19].

From nucleation theory [20], it is known that the nucleation barrier to form a spherical cluster depends on the cohesive forces between the atoms in the liquid phase, the energetic barrier due to the surface tension, and the plasma ionization (in dielectric materials the electric field leads to polarization). If the radius of the particles with packed atoms is very small, the particle will continue growing, while if it is large, the particle will stop growing and may even break up. The laser beam polarizes the atoms and this effect tends to pack them, so that the critical radius will be even smaller. So, the nucleation energy decreases and a higher amount of nuclei to generate the nanoparticles are produced [21].

Nucleation is said to be homogeneous if clusters are produced from the vaporized material, and the NPs are composed of a few tens of atoms. On the other hand, if clusters are already present during the vapor plume condensation, it is considered a heterogeneous condensation. The already existing clusters are considered nucleation centers and play a predominant role in the condensation stage.

The number of particles is decreased both by collisions and coalescence producing an increase of the NPs' average size. Coalescence in a vapor-liquid medium spontaneously occurs as a reduction of the total surface area during this process, corresponding to a reduction of Gibbs free energy. It takes place up to a few ms after the laser pulse. Then, the NPs cluster due to Van der Waals and electrostatic forces. Clustering is a characteristic feature of NPs' synthesis by laser ablation in gases or liquids that do not contain added stabilizing agents [21–24].

NPs suspended in transparent liquid media can be irradiated, too. Experiments show that when NPs' suspensions are irradiated with pulsed lasers, new structures [25] such as disks, segments, cubes, and pyramids of nanoscale dimensions [26–29] are generated.

## 2. Research methods

The nanostructures described in this chapter were found when machining micro-devices with a micromachining station based on laser ablation [30]. In particular, the monocrystalline silicon nanostructure was obtained in wafers coated with a sacrificial layer. The nanoparticles were found while analyzing the material ejected during the micro-devices' machining. Later, adequate containers for their generation were developed.

The micromachining station was composed of a laser and a substrates' positioning system. The laser was a frequency doubled Nd:YAG laser (532 nm) emitting pulses of 8 ns FWHM at

a repetition rate of 10 Hz. The maximum achievable fluence, for this wavelength, was 250 mJ/cm<sup>2</sup>. The substrates' positioning system consisted of eight motors: six stepper motors with micrometric resolution and two piezoelectric motors with nanometric resolution. A diagram of the micromachining station is shown in **Figure 1**.

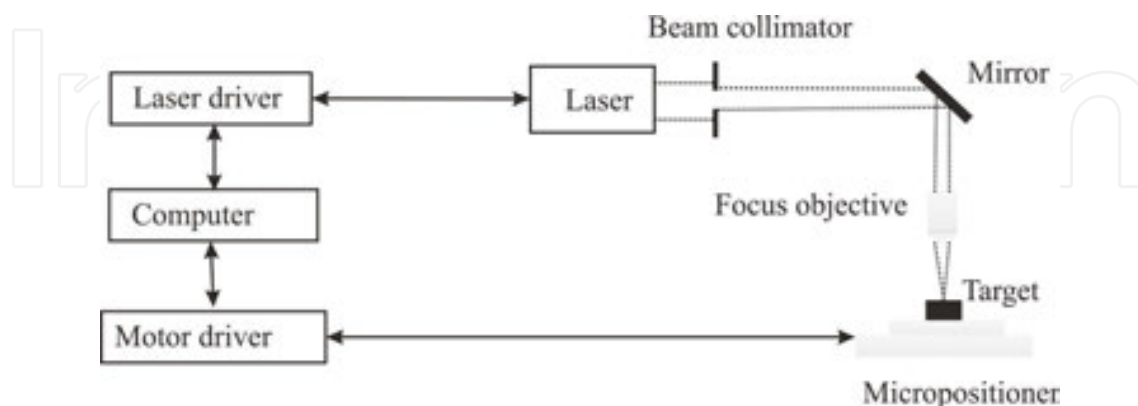


**Figure 1.** Micromachining system diagram.

Different samples of 2 cm × 2 cm of monocrystalline silicon were cut from c-Si wafers of 4" diameter and 525 μm thickness. These samples were later coated with different films: Si<sub>2</sub>O, Si<sub>3</sub>N<sub>4</sub>, positive photoresins, resins with dyes, or in some cases, a combination of these films.

The plasma-enhanced chemical vapor deposition (PECVD) technique [30–32] was used to perform Si<sub>2</sub>O and Si<sub>3</sub>N<sub>4</sub> films coatings. The effect of laser ablation on films of different thicknesses such as 110, 300, 430, 510, 1220, and 2400 nm was studied. The c-Si samples coated with Si<sub>2</sub>O were named c-Si + Si<sub>2</sub>O(*x*), where *x* indicates the film thickness in nm. The thicknesses of the Si<sub>3</sub>N<sub>4</sub> films were 180, 420, 500, 570, and 960 nm, and the naming: Si + Si<sub>3</sub>N<sub>4</sub>(*x*), *x* indicating the film thickness in nm. Commercial grade c-Si wafers were also used. These wafers have a 50 nm thick Si<sub>3</sub>N<sub>4</sub> film coating on either one or both sides.

Metals such as Fe (99.9%), Ag (99.9%), Au (99.9%), Ta (99.9%), and Cu were other materials processed. Results obtained on Tantalum coated with a 2.5 μm thick AZ1518 resin with the spin-coating technique [33] will be also presented.

## 2.1. Heuristic equation and its correlation with the physical properties of the irradiated substrate

Since the description of the different regimes observed in the ablation process was found to be a logistic function of the laser fluence, an ad hoc plasma detector was designed based on the works of Bredicce et al. [34] and M. Villagrán et al. [7]. This device, the working principles of which are detailed in reference [30], was used to detect the plasma during the machining. We found that for c-Si, the maximum value of the recorded signals was proportional to the amount of extracted material in each laser shot during the ablation regime according to references [7, 34]. **Figure 2** shows a plot of the induced electric signal maximum amplitude as a function of the incident fluence for c-Si and c-Si + SiO<sub>2</sub>(2400).



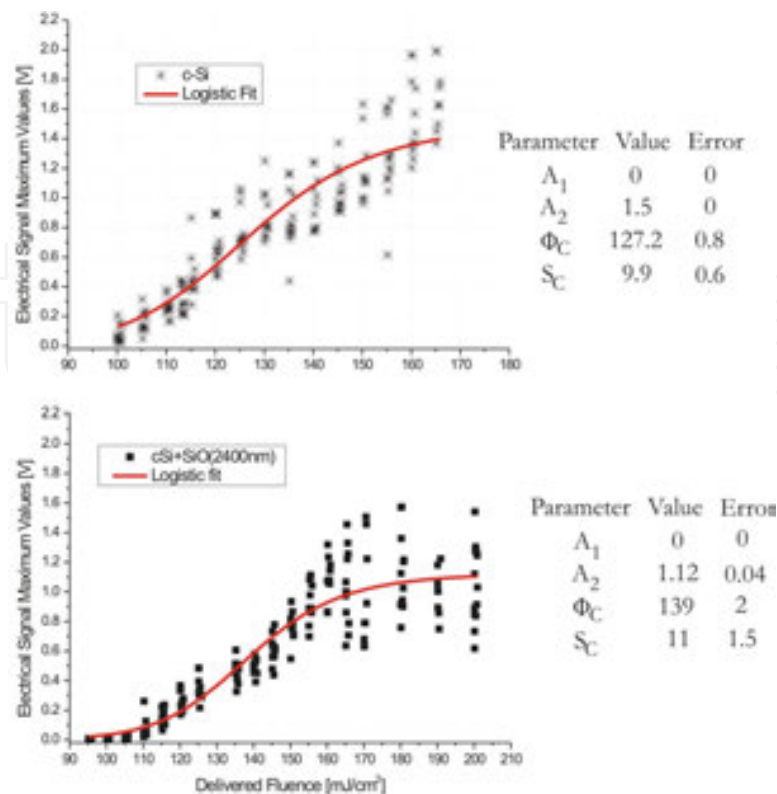


**Figure 2.** Amplitude of the electric signal versus laser fluence fitted by the logistic function of Eq. (1). (a) For c-Si and (b) for c-Si + SiO<sub>2</sub>(2400) along with the values of the fitting functions’ parameters.

The results were fitted with the heuristic function described by the following Eq.(1) that relates its parameters to the physical properties of irradiated substrates [34]:

$$M_J(\varnothing) = \left[ \frac{A_1(\varnothing) - A_2(\varnothing)}{1 + \left( \frac{\varnothing}{\varnothing_C} \right)^{S_C}} \right] + A_2(\varnothing) \tag{1}$$

where:

$M_J(\varnothing)$  is the amount of material removed per pulse which is proportional to the electric signal. Its units are [mass/(area)(time)], and it is a function of the laser fluence.

$\varnothing$  is in the laser fluence in mJ/cm<sup>2</sup>.

$A_1$  and  $A_2$  represent the lower and higher plateau values related to the onset of the absorption and ablation regimes, respectively. Their units are [mass/(area)(time)].

$S_C$  is a dimensionless fitting parameter related to the surface roughness.

$\varnothing_C$  is the critical fluence. Its value indicates the onset of the true ablation process, that is, the fluence value from which on the material removal occurs mainly through ablation. For

example, values of  $\varnothing_c = 127 \text{ mJ/cm}^2$  and  $\varnothing_c = 139 \text{ mJ/cm}^2$  were found for c-Si and c-Si +  $\text{Si}_2\text{O}(2400)$ , respectively (Figure 2).

Two plateaus were found for c-Si coated with thin films  $<1 \text{ }\mu\text{m}$ . We postulated that these values indicated whether the laser radiation had reached the substrate or not. Figures 3 and 4 show the results obtained for two different thicknesses of two kinds of films: c-Si +  $\text{Si}_3\text{N}_4(70)$  and c-Si +  $\text{Si}_3\text{N}_4(350)$ , and, c-Si +  $\text{SiO}_2(110)$  and c-Si +  $\text{SiO}_2(220)$ , respectively, along with the parameters' values.

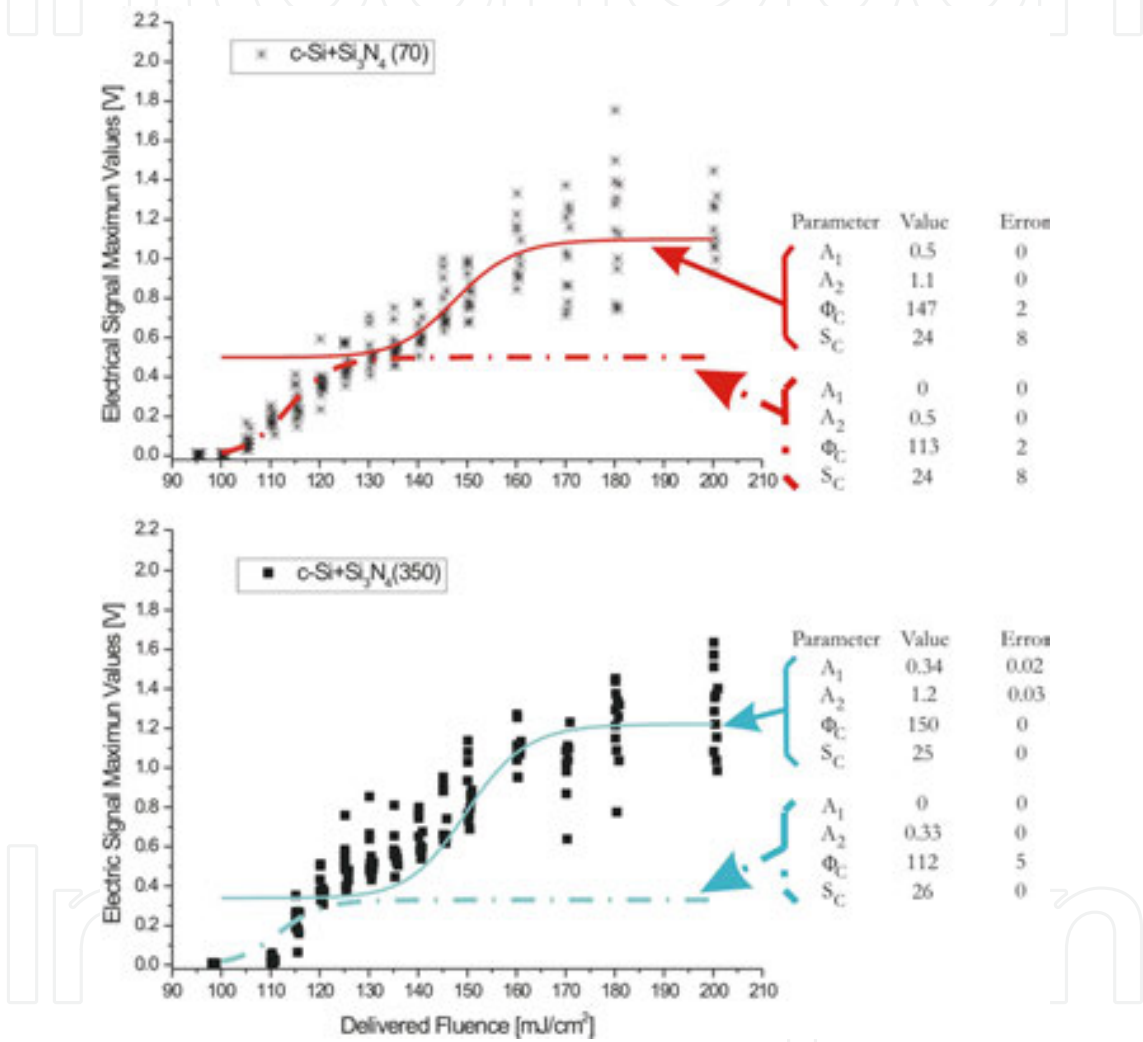


**Figure 3.** Amplitude of the electric signal versus laser fluence fitted by the logistic function, Eq. (1) for  $\text{Si}_3\text{N}_4$  thin films thicknesses deposited with the EPCVD technique on monocrystalline silicon: 70 and 350 nm. The parameters of the logistic function are shown too.

The fits show that the effect of the film is to change the surface roughness. This is evidenced by the value of the  $S_c$  parameter. The larger the value of this parameter, the lower is the roughness of the surface [7]. Thus, the film acts as a filter until the critical fluence,  $\varnothing_c$  is reached. At that moment, the material is ejected from the surface through ablation and generates a nanostructure on the substrate.

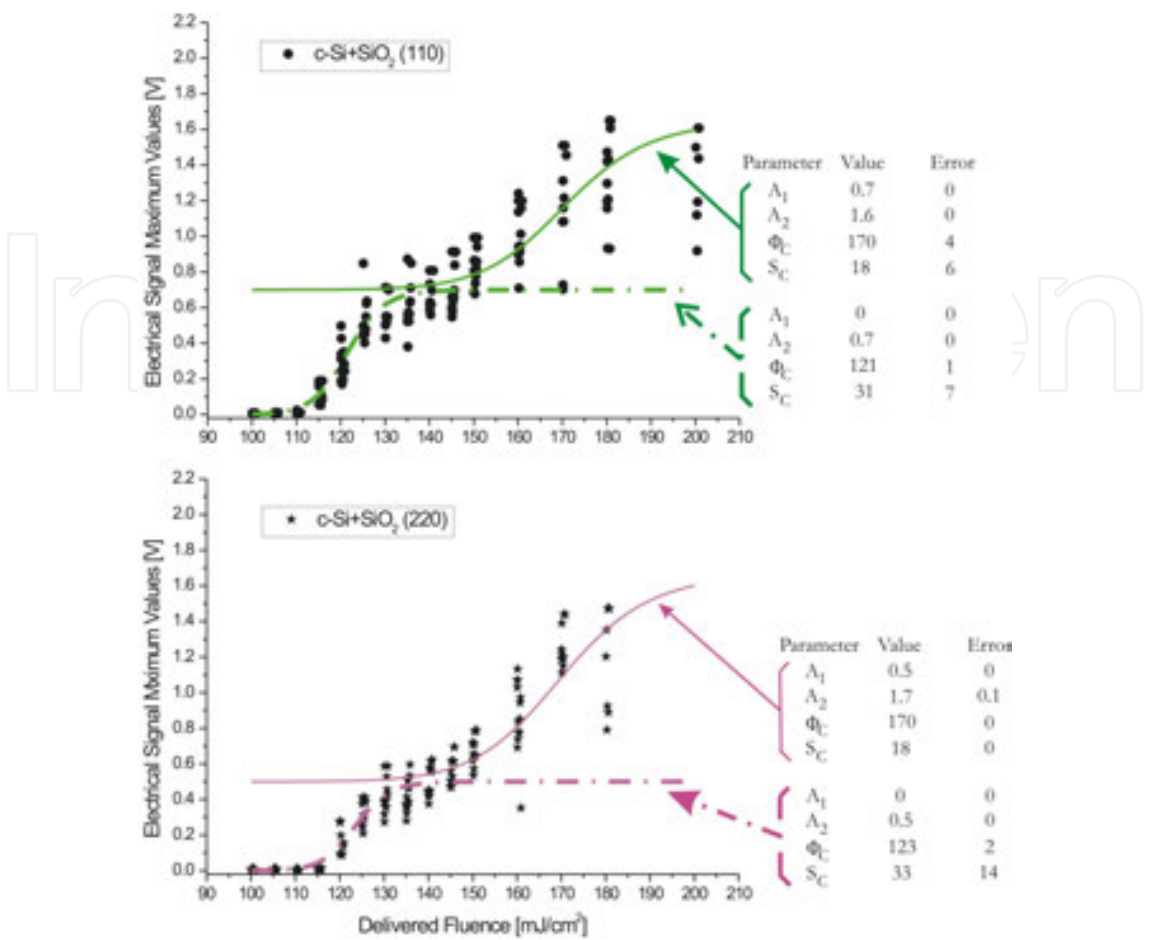


**Figure 4.** Amplitude of the electric signal versus laser fluence fitted by the logistic function, of Eq. (1) for two silicon dioxide thin films thicknesses deposited with the EPCVD technique on monocrystalline silicon: 110 and 220 nm. The parameters of logistic function are shown too.

## 2.2. Nanostructuring and nanoparticles manufacturing or generation

### 2.2.1. Nanostructuring on monocrystalline silicon (c-Si)

Nanostructuring on c-Si was observed during the manufacture of prototypes of nanopores and micro-cavities used as molecules' detectors, drug-delivery control, 2D microstructures, replication matrices, etc. in biological applications. These devices were manufactured using the following techniques in the specified order: (1) laser ablation micromachining (one laser shot cavities), (2) selective chemical attack, and (3) ultrasound cleaning (sonication) [35, 36]. The c-Si nanostructuring was observed after the ns laser pulse impacts on the c-Si + Si<sub>3</sub>N<sub>4</sub>(370) sample. The cavity formed and its nanostructured base can be observed in the SEM (scanning electron microscope) micrographies shown in **Figure 5**. c-Si nanostructuring has been reported in the literature only with sub-picosecond laser pulses [36–38]. The nanostructures produced in the irradiated zones reduce the reflection of the silicon surface. This effect would be of great interest in the manufacture of silicon photovoltaic cells.

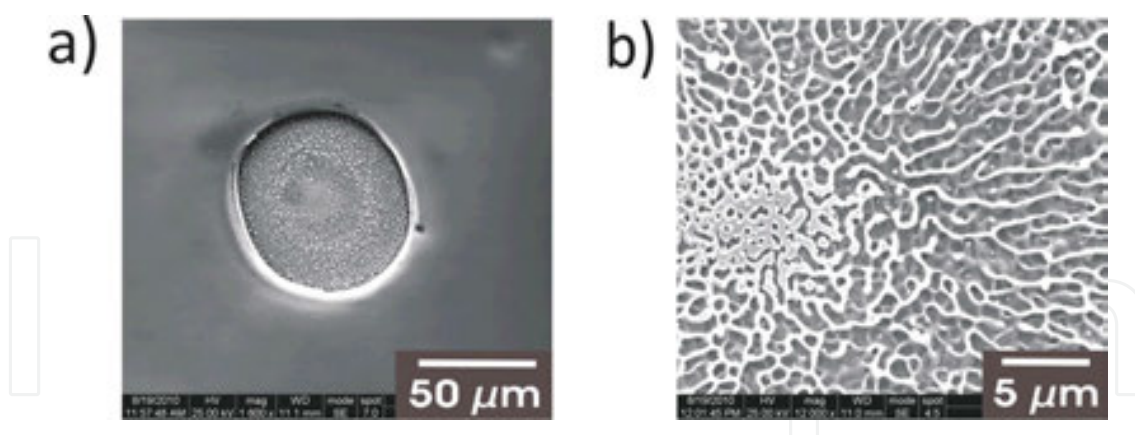


**Figure 5.** c-Si + Si<sub>3</sub>N<sub>4</sub>(370) nanostructuring obtained with a ns laser pulse (Nd:YAG, 8 ns, 532 nm). (a) Complete cavity. (b) Magnification of the cavity base.

Nanostructuring was also observed in the machining of a micro-chromatographic column in a c-Si + Si<sub>3</sub>N<sub>4</sub>(50) commercial wafer [30]. The roughness of the grooves, inherent to the c-Si—laser interaction—was found to be very useful to increase the sample concentration. The micro-column was manufactured as a sequence of straight lines. Part of this micro-chromatographic column and the roughness of the walls of the grooves is shown in **Figure 6**. The larger channels' depth was 50 μm. Devices used for separating substances require roughnesses similar to those of the sample's channels [39].

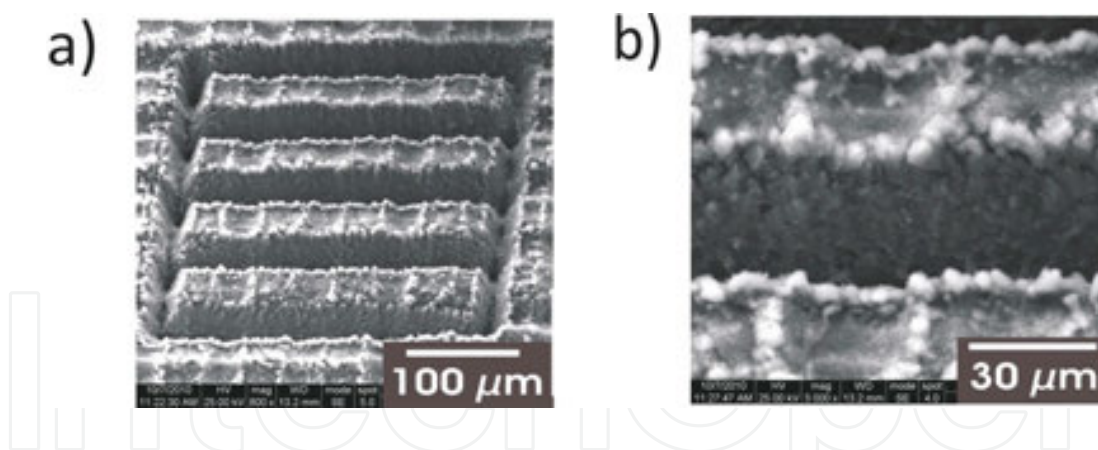


**Figure 6.** SEM microographies of (a) the c-Si sample surface after machining. (b) Magnification of part of the machined channels to show the deeper channels. In order to observe the roughness of the channel's wall, the sample's surface was placed forming an angle of 20° with electron beam.

Finally, microstructures and nanostructures were obtained on the walls of cylindrical and conical cavities. For this purpose, the machining station was used with either both percussion and trepanning drilling modes.

In the percussion drilling mode, the laser pulse always impacts in the same sample's area removing material until the desired depth is reached. Grooves of several microns width are obtained as can be seen in **Figure 7a**.

In the trepanning technique, a rotating movement is generated by applying sine wave voltages to the piezoelectric motors with coordinate phases associated to the XY axis of the positioning system. This circular nanometric movement produces a sand-down effect which decreases the drilled cavity walls' roughness. The misalignments of the laser beam focusing system as well as the beam's inhomogeneities are averaged and holes with controlled walls' shapes and roughness can be drilled. As a result, well-controlled circular holes with sub-micrometric structures on the wall can be drilled.

The SEM micrographies of **Figure 7** show cavities drilled on a sample of c-Si + Si<sub>2</sub>O(300) with different number of laser pulses of 110 mJ/cm<sup>2</sup>. A drilling performed with 2400 pulses with the percussion method can be seen in **Figure 7a**. The grooves on the walls and the debris can be also observed. The debris tower several microns over the silicon surface. A cavity drilled by trepanning with 200 pulses is presented in **Figure 7b**. Marks left by single pulses can be also seen on the sides. In this case, the field of view of electronic microscope allows observing the cavity bottom. Micrography (**Figure 7c**) corresponds to a cavity drilled by trepanning with 2000 laser pulses, the bottom of which can no longer be seen due to its depth. The walls of the cavities of **Figure 7b,c**, show the typical smoothness of the trepanning mode.

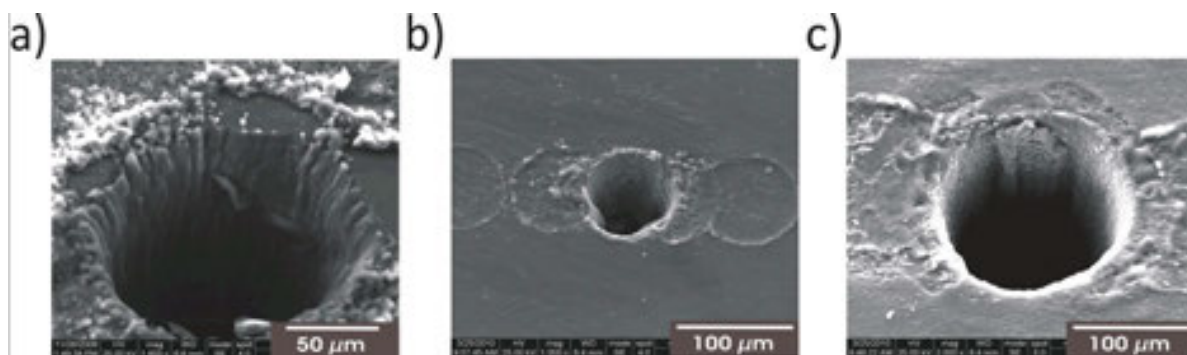


**Figure 7.** SEM micrographies of (a) c-Si wafer drilled by percussion with 2400 pulses. The sample was inclined 45° to observe the cavity's walls where grooves of ~10 µm are seen. (b, c) Micrographies of cavities drilled by trepanning with 200 and 2000 pulses, respectively. The effect of increasing the laser pulse number for a fixed sample-lens distance and a laser fluence of 110 mJ/cm<sup>2</sup> can be compared. A sine wave voltage of 10 V and 3 Hz was applied to the piezoelectric motors.

### 2.2.2. Nanostructuring in metals

The micromachining experiments in metals were performed with the machining station of **Figure 1**. Nanostructuring on the surface of the devices machined on metallic substrates was observed by electronic microscopy [30]. In this section, the most relevant results obtained are presented.

#### 2.2.2.1. Cavities in Ta(99.9%)

Porous tantalum is an alternative metal for the manufacture of total joint arthroplasty components that offer several unique properties since it has excellent biocompatibility and is safe to use in vivo [40]. Upon direct irradiation with several pulses impacting on the same area of



a Ta(99.9%) sample, formation of air bubbles of sub-micrometric dimensions gives rise to a porous coating of tantalum and tantalum oxide of the surface. **Figure 8** shows cavities drilled on a Ta sample with 1, 500, and 1000 laser pulses of  $200 \text{ mJ/cm}^2$ .

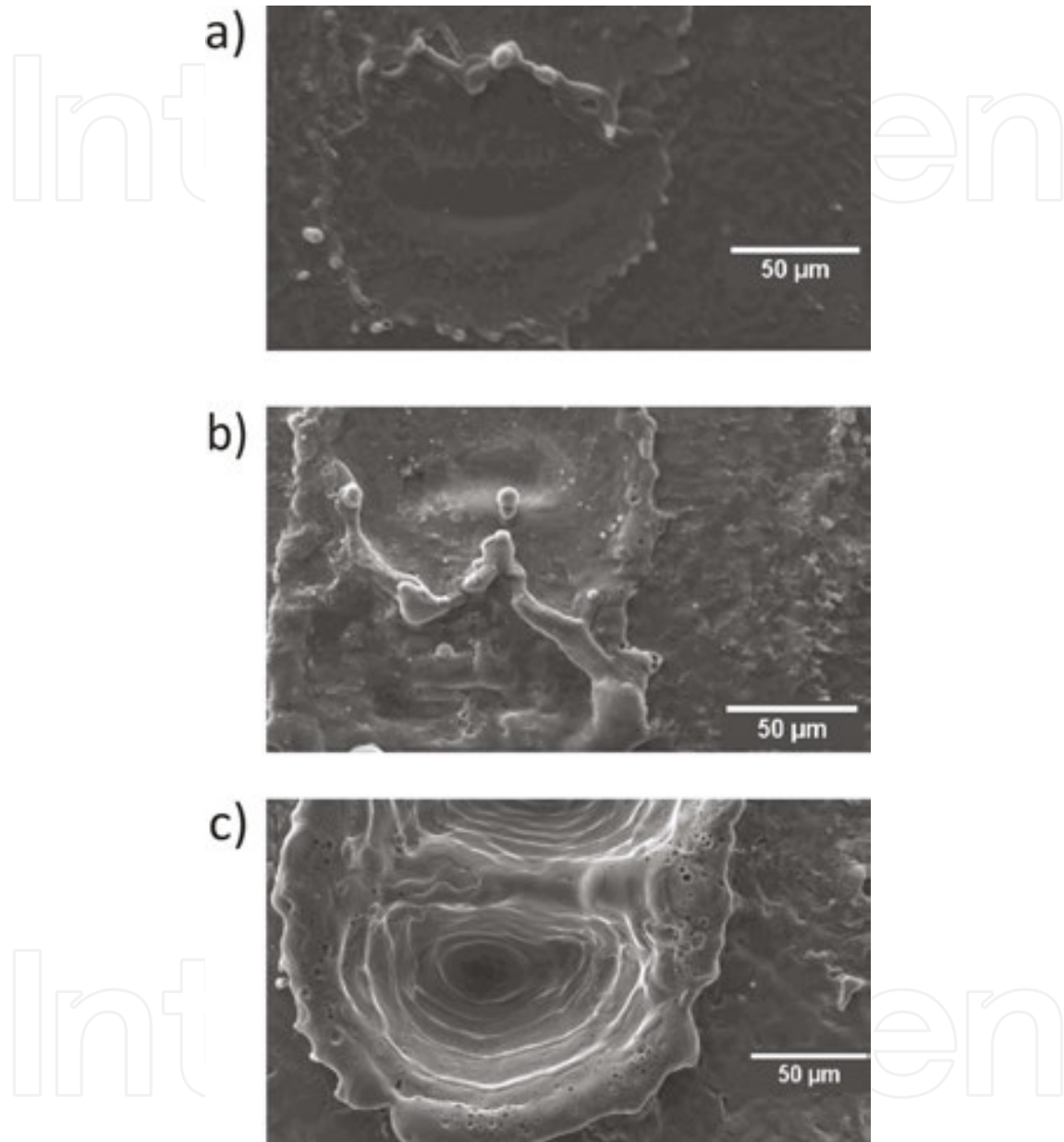


**Figure 8.** SEM micrographies of cavities drilled on a Ta(99.9%) sample with (a) 1, (b) 500, and (c) 1000 laser pulses of  $200 \text{ mJ/cm}^2$ .

#### 2.2.2.2. Nanostructuring in Cu

Micro-ionizer prototypes to be used in an ion mobility spectrometer [41] were machined on a printed circuit board (PCB). The thickness of the copper coating of these boards is about  $300 \text{ μm}$ . Direct irradiation of the Cu coating of the PCB was performed by the trepanning method

with 200 mJ/cm<sup>2</sup>. The SEM micrographies are shown in **Figure 9a**. It shows a sequence of contiguous cavities each drilled with 25 laser pulses each. **Figure 9b,c** shows the details of the cavities at different magnifications.

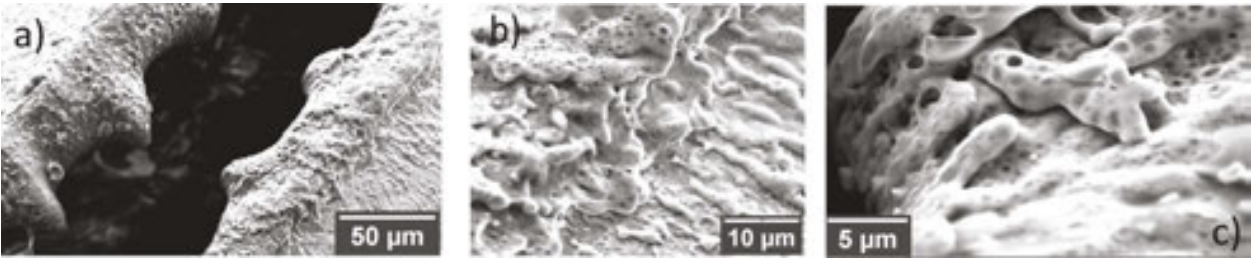


**Figure 9.** SEM micrographies (a) contiguous cavities machined on the copper coating of a PCB with 25 pulses each. (b, c) Micrographies at larger magnifications to show the porosity.

The appearance of a porous coating of copper and copper oxide is observed as the number of laser pulses impinging on the same sample area is increased. The lower density of porous copper makes it suitable to be used as a lighter material for electrodes and catalysis.

**Figure 10** shows the superficial modifications originated by laser irradiation of sub-micro-metric structures of copper oxide. **Figures 10a,b** are SEM micrographies of the surface before irradiation; **Figure 10c,d** after irradiation with one square laser shot.

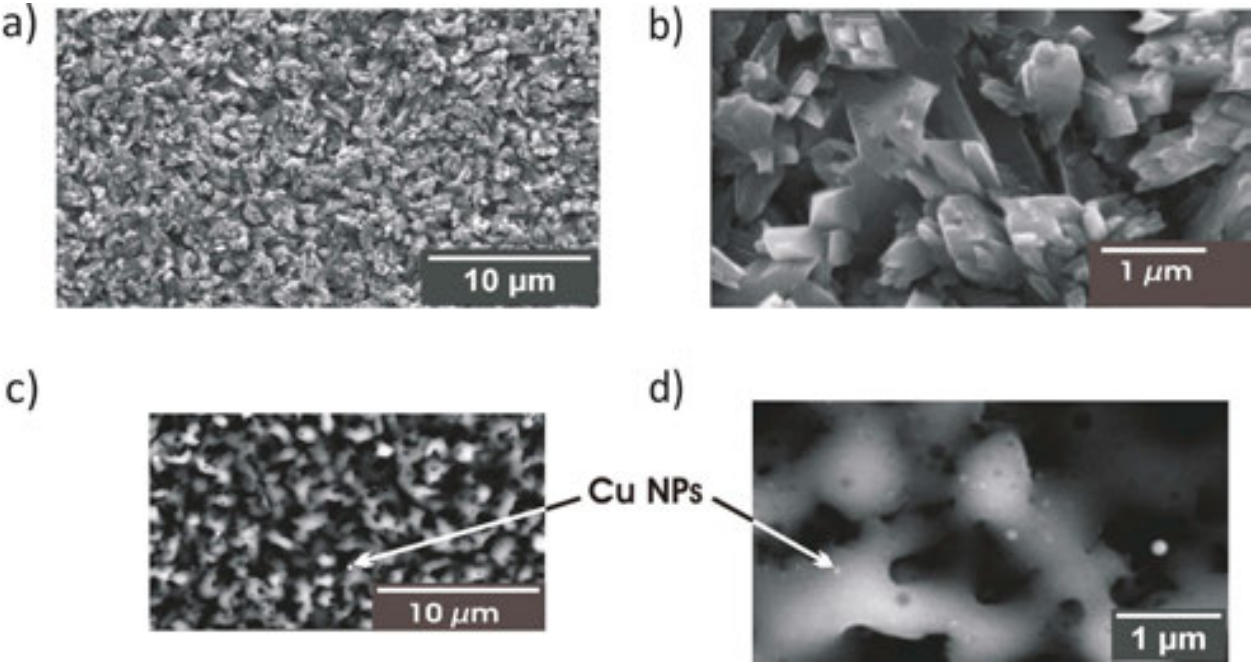


**Figure 10.** SEM micrographies of a copper oxide surface: (a, b) before irradiation; (c, d) after irradiation with one square laser shot. Cu nanoparticles of lighter color than the rest of the surface due to their larger conductivity can be appreciated.

### 2.2.2.3. Nanostructuring in Fe(99.9%)

The nanostructuring found in Ta and Cu encouraged the irradiation of Fe(99.9%) samples. Only sub-micrometric structures in Fe obtained with sub-picosecond laser pulses have been reported in the literature. The HAZ effect produced on the surface of steel plates is used as anticorrosive. In reference [41], Yang et al. report that the zones in the surroundings of a folding axis are more liable to corrosion due to the larger mechanical strains to which they are subjected. On the other hand, the authors found that steel plates which had been irradiated with laser pulses before being folded became more resistant to oxidation. **Figure 11** shows the surface of a Fe(99.99%) plate after irradiation with laser pulses of 200 mJ/cm<sup>2</sup> in which details of the induced surface nanostructuring can be observed.

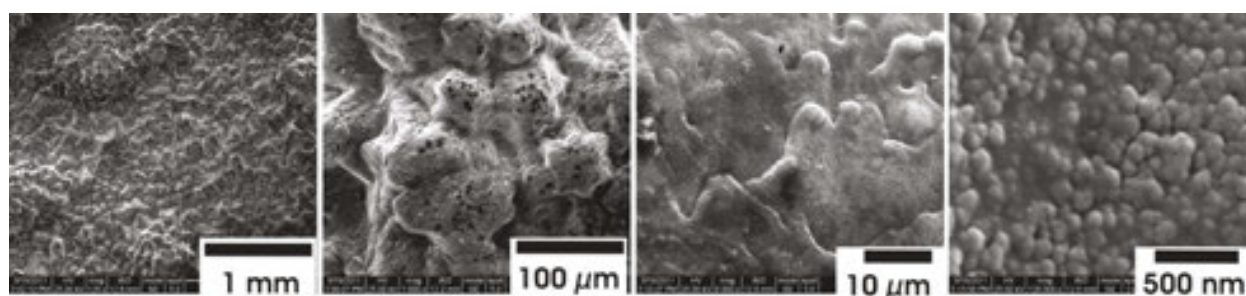


**Figure 11.** Fe (99.99%) plate surface after irradiation laser pulses of 200 mJ/cm<sup>2</sup>. The magnification of the electronic microscope (SEM) increases from left to right disclosing details of the surface nanostructuring.

### 2.2.3. Fe(99.9%), Au(99.9%), Ag(99.9%) nanoparticles in different media

The manufacture method of NPs of different metals and the diverse analysis performed will be described in the following. The first NPs were generated in air in an ad hoc chamber suitable for obtaining metallic NPs in gaseous media. The substrate was fixed to the container which was then fixed to the machining system. The laser was focused on the surface of the substrate, and the movement of the positioning system of the substrate was controlled by a PC. To ease the subsequent analysis with an electronic microscope, the NPs formed were stuck on carbon tapes.

**Figure 12** shows the Fe NPs generated in air at ambient temperature and pressure with two different irradiation processes. Those shown in **Figure 12a** were generated by drawing lines with a speed of 10 μm/s with pulses of 70 μm spot size. The irradiated zones and the number of pulses are detailed in **Figure 12b**. The NPs shown in **Figure 12c,d** were generated by drilling holes by percussion with 1000 pulses. The difference between both methods is the generation of clusters of NPs. The size of the NPs generated by overlapping pulses on the substrate's surface (**Figure 12a**) is ~200 nm, and, as can be seen, they are grouped in clusters. On the other hand, the size of the NPs generated by drilling is ~50 nm and they are also grouped in clusters. In addition to NPs clusters, the formation of dense spherical microparticles is observed (**Figure 12c**). This effect could be produced by the change of the superficial crystalline structure introduced by the ns 532 nm laser pulse on the metal surface, Fe(99.9%) in this case [43, 44].

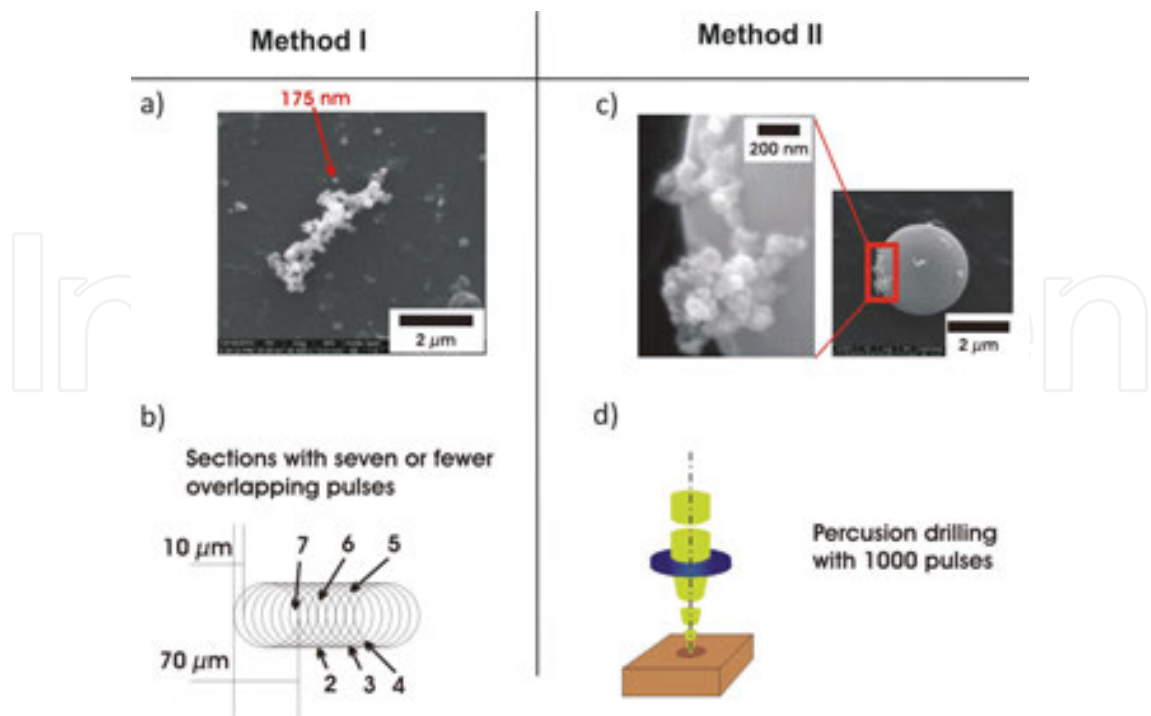


**Figure 12.** (a) Fe NPs manufactured by drawing lines with up to seven contiguous pulses, (b) Fe NPs generated by percussion (1000 pulses in the same sample area). In both processes, the laser fluence was 220 mJ/cm<sup>2</sup>. All micrographs were obtained by SEM.

The generation of NPs in liquid media was performed at ambient temperature and pressure. The substrate was immersed in the liquid contained in a beaker. Laser pulses were focused on the substrate’s surface, while the position of the substrate was continuously being changed so that each pulse would impact in a non-irradiated surface area. Metallic NPs dispersions in different liquid media such as ultrapure H<sub>2</sub>O, isopropanol, and a solution of sodium dodecyl sulfate (SDS) were obtained following this method.

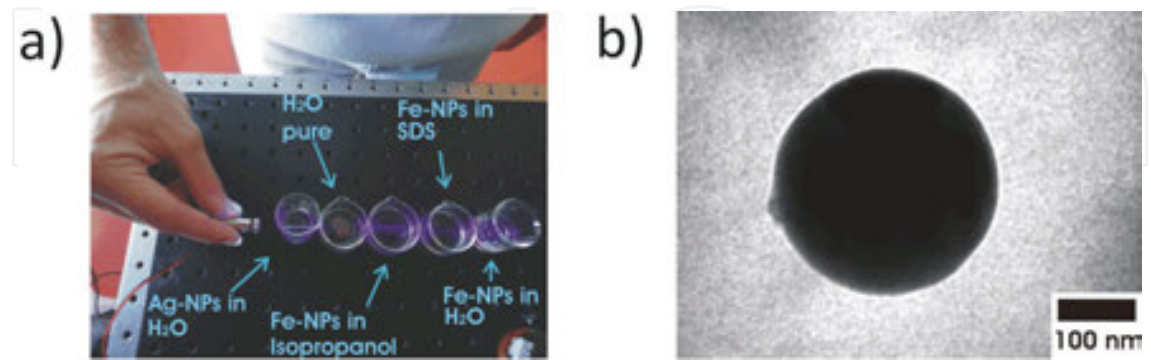


**Figure 13.** NPs generated in air and in different liquid media. (a) Tyndall effect in dispersions and solutions: (from left to right) Ag NPs in ultrapure H<sub>2</sub>O, ultrapure H<sub>2</sub>O, Fe NPs in isopropanol, Fe NPs in SDS, and Fe NPs in ultrapure H<sub>2</sub>O. (b) Characterization of the Fe NPs in a SDS solution by microscopy (HR-TEM).

Different methods were used for the NPs characterization:



1. Tyndall effect for a rapid verification of the NPs' generation in liquid media. In order to observe this effect, the dispersion is illuminated with a cw laser. For example, in **Figure 13a**, a 98 mW cw laser @405 nm was used. The presence of NPs disperses the laser beam and makes it visible at simple sight. This effect is not observed in solutions or as in the case of ultrapure H<sub>2</sub>O in the second beaker from left to right of **Figure 13a**.
2. High-resolution transmission electron microscopy (HR-TEM), which allowed studying the NPs' appearance, form and size (**Figure 13b**).
3. UV-visible light absorption spectrophotometry for the analysis of suspensions.

The advantage of this last method is that it allows preserving the NPs' properties *in situ*, avoiding alterations due to drying effects. Clustering or oxidation effects usually appear when the NPs are separated from the medium in which they were originated (**Figure 14**).

Finally, the size distribution of the NPs in their original medium was estimated from the absorbance spectra of the dispersions and their comparison with those calculated with the MiePlot algorithm (Appendix E, reference [30]).

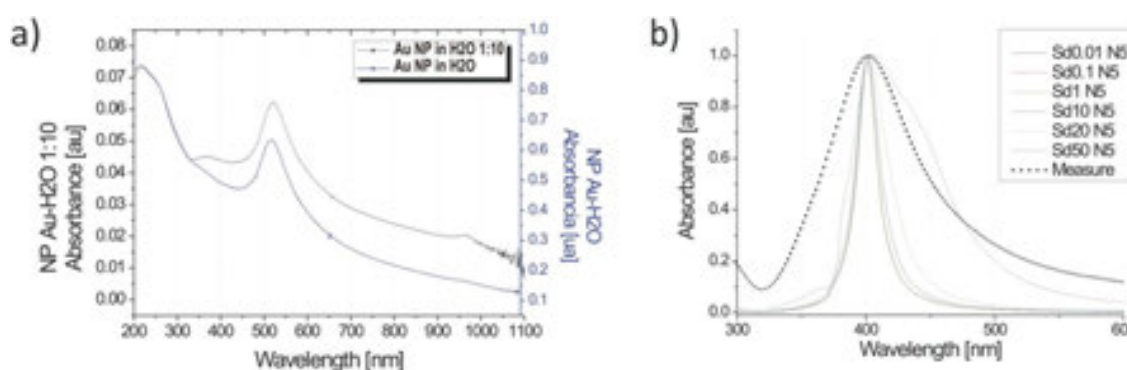


**Figure 14.** (a) Absorbance spectrum of a dispersion of Au NPs in ultrapure H<sub>2</sub>O compared to that of the same dispersion diluted 10 times, (b) comparison of the absorbance spectrum of Ag NPs in H<sub>2</sub>O experimentally obtained with that calculated for Ag NPs of 20 nm of radius in H<sub>2</sub>O with a log-normal distribution with different standard deviations.

#### 2.2.3.1. Core-shell nanoparticles (preliminary results)

Nanoparticles of different nucleus' materials and *core-shell* were produced as prototypes for *drug delivery*. The particles were required to have a ferromagnetic nucleus to be able to be delivered with magnets to the desired zones and a *core-shell* of a material assimilable by the organism so as not to be rejected by it.

The following method was used for the synthesis of *core-shell* NPs. First, a suspension of Fe NPs in ultrapure H<sub>2</sub>O was obtained by laser ablation of a Fe(99.9%) plate. An Au(99.9%) plate was subsequently irradiated in the Fe NPs suspension. The Fe NPs acted as nucleation centers for Au crystallization according to the nucleation principles described in Section 1.1.1.2.

The absorbance spectrum of the final suspension obtained, shown in **Figure 15**, resulted in very good agreement with those reported by other authors in references [45, 46].



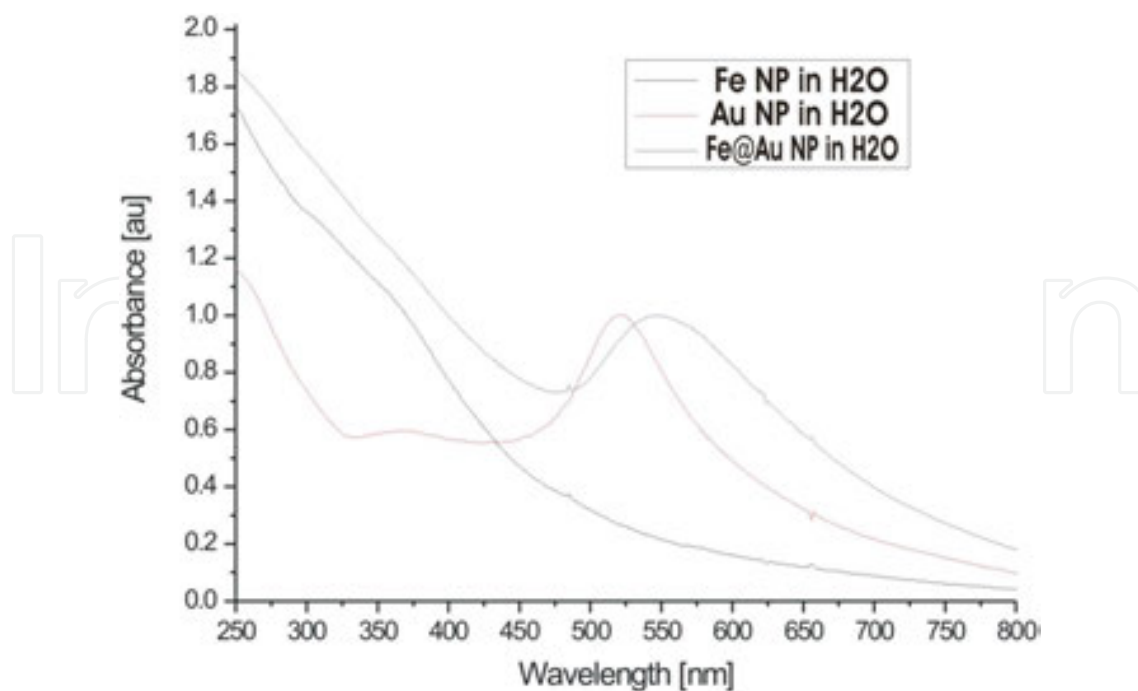


**Figure 15.** Absorbance spectrum of dispersions of Fe NPs, Au NPs, and Fe@Au NPs in ultrapure H<sub>2</sub>O.

### 3. Conclusions

Laser ablation allows numerous technological developments ranging from laser-induced breakdown spectroscopy (LIBS), pulsed laser deposition (PLD), laser propulsion, to surface modification and generation of nanoparticles, NPs. In this chapter, we have presented a review of the results obtained with these two latter processes. However, it should be noted that these effects or phenomena were found to occur during the implementation of the micromachining processes and have gained relevance since their observation by means of electron microscopy in its different forms SEM and TEM. The possibility of producing nanostructures on surfaces opens up new possibilities for studying their effects on physicochemical surface phenomena. These effects, mentioned in the Section 1.1.1, as laser-induced periodic surface structures and the increase of roughness in the generation of channels for chromatographic columns will allow the production of cheaper systems based on these principles. On the other hand, the heuristic model presented in Section 2.1 to explain the phenomenon of laser ablation allows us to understand the effect of surface modification and use it as a tool to transform surfaces by coating them with thin films. Another very important issue is the possibility of producing core-shell nanoparticles of the type shown in the Section 2.2, using different metals. In our case, the production of Fe@Au NPs resulted a very convenient way to unify in a same material the magnetic properties of Fe with the biological properties of Au. As a final remark, as it was our intention to put forward throughout this chapter, we would like to emphasize that nanosecond lasers are still a very important source for the modification of surfaces for technological uses.

## Author details

Cinthy Toro Salazar<sup>1</sup>, María Laura Azcárate<sup>1,2</sup> and Carlos Alberto Rinaldi<sup>2,3,4\*</sup>

\*Address all correspondence to: [rinaldi@cnea.gov.ar](mailto:rinaldi@cnea.gov.ar)

1 Centro de Investigaciones en Láseres y Aplicaciones CEILAP (CITEDEF-CONICET), Buenos Aires, Argentina

2 Consejo Nacional de Investigaciones Científicas Técnicas, Buenos Aires, Argentina

3 Comisión Nacional de Energía Atómica, Buenos Aires, Argentina

4 Escuela de Ciencia y Tecnología, UNSAM, Buenos Aires, Argentina

## References

- [1] K. Sugioka, M. Meunier and Alberto Piqué. Laser Precision Microfabrication. Springer Series in Materials Science. 2010.
- [2] N.B. Dahotre and S.P. Harimkar. Laser Fabrication and Machining of Materials. Springer. 2008.
- [3] W. M. Steen. Laser Material Processing. Springer-Verlag. 1991.
- [4] E. Gentili, L. Tabaglio and F. Aggogeri. Review on Micromachining Techniques. Italy: Department of Mechanical Engineering, University of Brescia. 2005.
- [5] M.B. Mason (BP Solar) and J. Fieret (Exited Ltd). Advanced Laser Processing for Industrial Solar Manufacturing. Contractor BP Solar Limited. 2006.
- [6] M.M.S. Amara, M.A. El-Ashrya, L.R. Dosserb, K.E. Hixb, J.F. Maguirec and B. Irwin. Femtosecond versus nanosecond laser machining: comparison of induced stresses and structural changes in silicon wafers. Applied Surface Science. 2005;242:162–167.
- [7] M. Villagran-Muniz, H. Sobral, C. Rinaldi, I. Cabanillas-Vidosa and J. Ferrero. Optical emission and energy disposal characterization of the laser ablation process of CaF<sub>2</sub>, BaF<sub>2</sub>, and NaCl at 1064 nm. Journal of Applied Physics. 2008;104:103112–103117.
- [8] C. Toro, C. Lasorsa, C. Sánchez Aké, M. Villagran-Muñiz and C. Rinaldi. New method for nanosecond laser machining. Journal of Laser Micro Nanoengineering. 2012;7:269–273.
- [9] J. Eichstädt, G.R.B.E. Römer and A.J. Huisin 't Veld. Determination of irradiation parameters for laser-induced periodic surface structures. Applied Surface Science. 2013;264:79–87.

- [10] W. Zhang, G. Cheng, Q. Feng, L. Cao, F. Wang and R. Hui. Abrupt transition from wavelength structure to subwavelength structure in a single-crystal superalloy induced by femtosecond laser. *Applied Surface Science*. 2011;257:4321–4324.
- [11] R. Le Harzic, D. Dörr, D. Sauer, M. Neumeier, M. Epple, H. Zimmermann and F. Stracke. Formation of periodic nanoripples on silicon and germanium induced by femtosecond laser pulses. *Physics Procedia*. 2011;12:29–36.
- [12] T.Q. Jia, H.X. Chen, M. Huang, and F.L. Zhao, J.R. Qiu, R.X. Li and Z.Z. Xu, X. K. He, J. Zhang and H. Kuroda. Formation of nanogratings on the surface of a ZnSe crystal irradiated by femtosecond laser pulses. *Physical Review B*. 2005;72:125429.
- [13] Available from: <http://www.nasa.gov/centers/ames/research/technologyonepaggers/nanotechnology-landing.html>.
- [14] Available from: [http://www.cnea.gov.ar/institutos/nanociencia\\_nanotecnologia.php](http://www.cnea.gov.ar/institutos/nanociencia_nanotecnologia.php).
- [15] Available from: <http://www.fan.org.ar>.
- [16] T.H. Maiman. *Nature*. 1960;187:493.
- [17] G. Bekefi. *Principles of Laser Plasmas*. 1st ed. New York: Wiley. 1976.
- [18] F. Hubenthal. Vol. 1, Sección 1.13. In: *Comprehensive Nanoscience and Technology*. 2011;375–435.
- [19] D. Kashchiev. *Nucleation: Basic Theory with Applications*. Oxford: Butterworth-Heinemann. 2000.
- [20] B.S. Luk'yanchuk, W. Marine, S.I. Anisimov and G.A. Simakina, Condensation of vapor and nanoclusters formation within the vapor plume, produced by ns-laser ablation of Si, Ge and C, *Proc. SPIE* 3618, 434. 1999.
- [21] M.S. Tillack, D.W. Blair and S.S. Harilal. The effect of ionization on cluster formation in laser ablation plumes. *Nanotechnology*. 2004;15:390–403.
- [22] J. Perrière, É. Millon, É. Fogarassy, A.V. Kabashin and M. Meunier. *Recent advances in laser processing of materials*. Amsterdam: European Materials Research Society: Elsevier. 2006.
- [23] R. Hergenroder. Laser-generated aerosols in laser ablation for inductively coupled plasma spectrometry. *Spectrochimica Acta Part B: Atomic Spectroscopy*. 2006;61(3).
- [24] P.S. Liu, W.P. Cai and H.B. Zeng. *Journal of Physical Chemistry C*. 2008;112:3261.
- [25] K.Y. Niu, J. Yang, S.A. Kulinich, J. Sun, H. Li and X.W. Du. *Journal of the American Chemical Society*. 2010;132:9814.
- [26] Z. Yan and D.B. Chrisey. Pulsed laser ablation in liquid for micro-/nanosstructure generation. *Journal of Photochemistry and Photobiology C: Photochemistry Reviews*. 2010;doi:10.1016/j.jphotochemrev.2012.04.004.

- [27] D. Werner, S. Hashimoto, T. Tomita, S. Matsuo and Y. Makita. *Journal of Physical Chemistry C*. 2008;112:1321.
- [28] Z.J. Yan, R.Q. Bao and D.B. Chrisey. *Langmuir*. 2011;27:851.
- [29] A.V. Simakin, V.V. Voronov, G.A. Shafeev, R. Brayner and F. Bozon-Verduraz. *Chemical Physics Letters*. 2001;348:182.
- [30] C.T. Salazar. *Micromecanizado por ablación láser en silicio, en silicio cubierto por películas y en metales* [thesis]. Buenos Aires, Argentina: Facultad de Ingeniería, Universidad de Buenos Aires. 2015;129 p.
- [31] C. Toro, C. Lasorsa and C. Rinaldi. Detecting plasma produced by laser in a micromachining system as in-process control. *Journal of Laser Micro Nanoengineering*. 2011;6:220–224.
- [32] A. Rodrigo, et al. Dominant plasma species for TiN film formation by plasma CVD. *Journal of Physics D: Applied Physics*. 1997;30:2397.
- [33] Spin coating theory. Louisville: Micro/Nano Technology Center, University of Louisville. 2013.
- [34] H. Sobral, M. Villagrán-Muniz and F. Bredice. Energy balance in laser ablation of metal targets. *Journal of Applied Physics*. 2005;98:083305.
- [35] B. Lerner, M. Perez, C. Toro, C. Lasorsa, C.A. Rinaldi, A. Boselli and A. Lamagna. Generation of cavities in silicon wafers by laser ablation using silicon nitride as sacrificial layer. *Applied Surface Science*, Amsterdam: Elsevier Science BV. 2012;258:2914–2919.
- [36] M. Halbwaxa, T. Sarneta, Ph. Delaporte, M. Sentisa, H. Etienneb, F. Torregrosab, V. Vervischb, I. Perichaudc and S. Martinuzzic. Micro and nano-structuration of silicon by femtosecond laser: application to silicon photovoltaic cells fabrication. doi:10.1016/j.tsf.2007.12.117.
- [37] T. Baldacchini, J.E. Carey, M. Zhou and E. Mazur. Superhydrophobic surfaces prepared by microstructuring of silicon using a femtosecond laser. *Langmuir*. 2006;22:4917–4919.
- [38] B.R. Tull, J.E. Carey, E.Mazur, J.P. McDonald and S.M. Yalisove. Silicon surface morphologies after femtosecond laser irradiation. *Mrs Bulletin*. 2006;31:626–633.
- [39] E.H.M. Camara, P. Breuil, D. Briand, L. Guillot, C. Pijolat and N.F. de Rooij. Review: Micro gas preconcentrator in porous silicon filled with a carbon absorbent. *Sensors and Actuators B*. 2010;148:610–619.
- [40] B. Levine, C.J. Della Valle and J.J. Jacobs, Applications of porous tantalum in total hip arthroplasty. *Journal of the American Academy of Orthopaedic Surgeons*. 2006;14(12): 646–655.

- [41] N.G. Boggio, P. Alonso Castillo, J.J. Ortiz, A. Lamagna, A. Boselli and C.A. Rinaldi. Desarrollo de un espectrómetro por movilidad iónica para la detección de compuestos orgánicos (explosivos, drogas y contaminantes). *Anales AFA*.
- [42] L.J. Yang, J. Tang, M.L. Wang, Y. Wang and Y.B. Chen. Surface characteristic of stainless steel sheet after pulsed laser forming. *Applied Surface Science*. 2010;256:7018–7026.
- [43] C. Toro, E.D. Cabanillas and C.A. Rinaldi. New method for micro and nanoparticles fabrication. In: Japan Laser Processing Society, editor. *The 12th International Symposium on Laser Precision Microfabrication*; Japan, Takamatsu, Kagawa. 2011.
- [44] C. Toro, E.D. Cabanillas and C.A. Rinaldi. Generación de nanopartículas y modificación de superficies de Fe con ablación láser. In: Instituto de Química del Noroeste Argentino, editor. *XVII Congreso Argentino de Fisicoquímica y Química Inorgánica*; Argentina. Córdoba. 2011.
- [45] S. Kayal and R.V. Ramanujan. Anti-cancer drug loaded iron–gold core–shell nanoparticles (Fe@Au) for magnetic drug targeting. *Journal of Nanoscience and Nanotechnology*. 2010;10:1–13.
- [46] *Journal of Magnetism and Magnetic Materials*. 2007;310:2369–2371.